RESEARCH METHODS

No-touch measurements of vital signs in small conscious animals

Xiaonan Hui* and Edwin C. Kan

Measuring the heartbeat and respiration of small conscious animals is important for assessing their health and behavior, but present techniques such as electrocardiogram (ECG), ultrasound, and auscultation rely on close skin contact with the animal. These methods can also require surface preparation, cause discomfort or stress to animals, and even require anesthetic administration, especially for birds, reptiles, and fish. Here, we show that radio frequency near-field coherent sensing (NCS) can provide a new solution to animal vital sign monitoring while ensuring minimal pain and distress. We first benchmarked NCS with synchronous ECG on an anesthetized rat. NCS was then applied to monitor a conscious hamster from outside its cage, and was further extended to a parakeet, Russian tortoise, and betta fish in a noninvasive manner. Our system can revolutionize vital sign monitoring of small conscious animals in their laboratory living quarters or natural habitats.

INTRODUCTION

In this paper, we demonstrate a new touchless method to measure the vital signs of small conscious animals, where the near-field coherent sensing (NCS) principle is applied to previously unachievable sensing ability and testing convenience. Our setup has minimal interference to the daily rhythms of the animal under test; most subjects will likely not even notice the ongoing real-time measurement. With this work, we not only provide an innovative tool to facilitate small-animal studies but also promote refinement in animal laboratory procedures against invasive, risky, and sometimes inhumane techniques such as anesthetization, hair/scale removal, forceful body stretch, intramuscular electrode insertion, and surgical implants.

Difficulties in present methods

Current approaches to measuring vital signs in animals with various body coverings often involve complicated and invasive preparation procedures (*1, 2*) and cause major distress to the animals, even requiring that they be anesthetized or heavily restrained to prevent motion that could disrupt the measurement setup. For example, an electrocardiogram (ECG) (*2–5*) for heartbeat waveforms requires skin electrodes with stable electrical contact and is therefore difficult to be applied to mammals with thick fur, reptiles with scutes or shells, birds with feathers, and fish with scales. Bare skin areas such as soles and lips often have insufficient electrical signals and can be sensitive to touch. Intramuscular electrodes are typically performed with anesthetization. Similarly, the body surface condition also causes intricacy in photoplethysmography (PPG) (*6, 7*), which limits its application to animals. Auscultation (*8, 9*) and ultrasound (*10, 11*) need tight skin touch or impedance-matching gels to obtain clear signals, which require high degrees of animal handling. Radio frequency (RF) methods such as Doppler far-field backscattering (*12–16*) of minute skin motion have nonspecific wireless channels and can be potentially interfered by ambient motion covered by the same beam lobe, although beamforming by large antenna arrays can improve directivity at the cost of system complexity. To be sufficiently sensitive to the vital signs of small animals, raising the carrier

frequency to the millimeter-wave level was proposed (*17, 18*), which not only increases the system cost but also reduces the operational distance. Respiration can often be the dominant signal and become a major interference to accurate heartbeat detection. RF methods based on the transmission line model (*19–21*) again require good impedance matching of the skin electrodes and hence the associated surface preparation. Small animals pose further challenges for most of these previous RF methods because of their limited signal sensitivity.

Experimental setups

Our recently proposed NCS method (*22*) by near-field modulation of the antenna characteristics on multiplexed radio signals has very high signal-to-noise ratio (SNR) but does not require restraint or even contact with the animal (*23*). NCS thus offers an effective solution to long-term vital sign monitoring for small conscious animals with various body coverings. The schematics for two possible NCS setups are shown in Fig. 1. The wireless sensing in Fig. 1A uses the harmonic RFID (radio frequency identification) architecture (*24*), where the passive sensing tags are inexpensive and maintenance free, but a specific multiplexing reader (*25*) is required. This version can be appropriate for deployment in natural habitats with weather-proof passive tags, and the vital signs are collected from a nearby reader on the operator or fixture. To retrieve accurate vital signs of small animals, the system SNR and sensitivity are critical because of the weak signal strength from a very small motion source. The conventional RFID system uses the same frequency band for the transmitter (Tx) and receiver (Rx). Thus, the Tx-to-Rx leakage, the antenna reflection caused by antenna impedance mismatch, and the ambient reflection from nearby large objects are received and amplified by the Rx chain together with the intended signals carrying the vital signs. Considering the double-trip path loss and available scavenged power of the passive tag, not only is the amplitude of the tag signal at Rx weak but also the sideband frequency offset is small, with low base bandwidth. The backscattering from tags can be easily overwhelmed by the phase noise skirt of the Tx leakage or the reflected carrier signal to render poor SNR and signal sensitivity.

The use of the harmonic system reduces self-jamming by separating the bands of Tx and Rx and improves both SNR and signal sensitivity. The NCS signal impinged on the animal body is estimated

School of Electrical and Computer Engineering, Cornell University, Ithaca, NY 14853, USA.
*Corresponding author. Email: xh273@cornell.edu
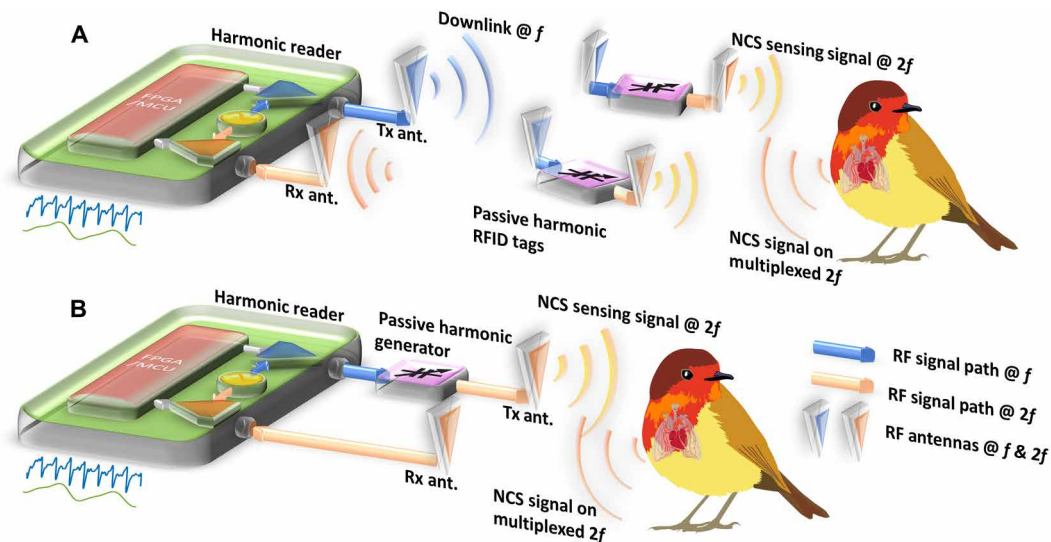
Fig. 1. Two setups of NCS for vital signs of small conscious animals. The signal is collected by the harmonic reader with digital baseband processing by the field-programmable gate array (FPGA) and microcontroller (MCU). (**A**) The wireless NCS system is realized by the harmonic RFID system with passive harmonic sensing tags. (**B**) The wired NCS system replaces the wireless links between the reader and the harmonic tag by RF cables for reduced interference and convenient indoor laboratory deployment.

to be much lower than 0.1 mW/cm^2 and 0.15 W/kg to comply with the health and safety standards in the human and rodent models (*26*). In Fig. 1A, the harmonic reader by Ettus X310 Software Defined Radio (SDR) transmits the downlink signal at *f* around 950 MHz (the blue wave) through the reader Tx antenna. The downlink signal powers up the passive harmonic RFID tags and is then converted to the second-harmonic frequency at 2*f* as the NCS sensing signal (the yellow waves) in the vicinity of the target animal body. As long as the vital signals are within the near-field range (typically about one-third of the used wavelength) of the sensing tag antenna, motion on and inside the animal body can be coupled to the backscattered signal (the orange wave) to be received by the reader Rx antenna. The overall tag antenna motion relative to the reader Rx will be mostly represented by phase modulation, which can be naturally separated from the magnitude modulation out of the dielectric boundary motion relative to the tag antenna in the near field. The signal originated from the sensing tag can contain a unique identification code to achieve code-division multiple access (CDMA) (*25*), which improves channel isolation against nonspecific interference and enables simultaneous reading of multiple sensing tags. Manufacturing of the passive sensing tag is similar to the conventional RFID tag, which gives low-cost production (*27*) and flexible substrate choices (*28*) in addition to convenient deployment without need of maintenance.

Alternatively, the setup in Fig. 1B replaces the reader-to-tag channels with RF cables, which reduces interferences and can be appropriate for convenient deployment in an indoor laboratory with heavy operator traffic or with other interfering sources. The reader Tx antenna transmits the NCS sensing signal (the yellow wave) directly at 2*f* and is in the near-field range of the animal under test. Then, the NCS signal modulated by the vital signs (the orange wave) is received by the reader Rx antenna, which can be deployed according to the application under consideration. The use of 2*f* here is mainly to reduce the Tx-to-Rx leakage inside the SDR. When sufficient Tx-to-Rx isolation can be achieved by improved transceiver design, the harmonic scheme to separate Tx and Rx bands becomes optional. Because the ambient interference is reduced and no tag circuit needs to be supported by scavenged power, the Tx NCS signal to couple into the animal body can be further decreased to eliminate any health concerns of RF radiation.

RESULTS AND DISCUSSION
Benchmarks on an anesthetized rat
To compare the NCS vital signals on small animals for cardio waveforms, we first performed synchronized NCS and ECG measurements on an established rodent model, which not only is important for pharmaceutical trials but also has much fainter and faster heartbeats than humans, providing a more challenging test. A Long-Evans laboratory rat (*Rattus norvegicus*), coded #110, was anesthetized with complete belly hair removal by razors and Veet gel cream for ECG electrode deployment, as shown in Fig. 2A. We also tried out alligator clips and conductive sticker pads on both paws, but the ECG signal was much weaker and noisier. The sensing tag antenna with the architecture in Fig. 1B was placed near the back of the neck area by a rubber harness without hair removal. Other antenna placements, including along the tail, in front of the chest, and along the back leg, were also attempted with reasonable NCS signal strength. A representative 5-min recording is shown in Fig. 2A, and the inset shows the waveform details within half a second within the third minute. The cardiogram waveforms of ECG and NCS in Fig. 2B rendered very similar beat-to-beat intervals (*26*), as shown in Fig. 2C. However, the detailed waveforms, for example, the NCS feature points in comparison with the ECG S and T feature points, will need further characterization. In view of heart rate comparison, NCS is sufficiently accurate to replace ECG for behavior studies based on heart rate variation (HRV). The breath waveforms were synchronously collected by NCS with an additional 0.5- to 2.5-Hz low-pass filtering in Fig. 2D, allowing further cardio-pulmonary analyses not achievable by ECG alone.

NCS measures the tag antenna characteristics modulated by the near-field dielectric boundary movement changes, while ECG measures the body potential differences induced by the minute skin
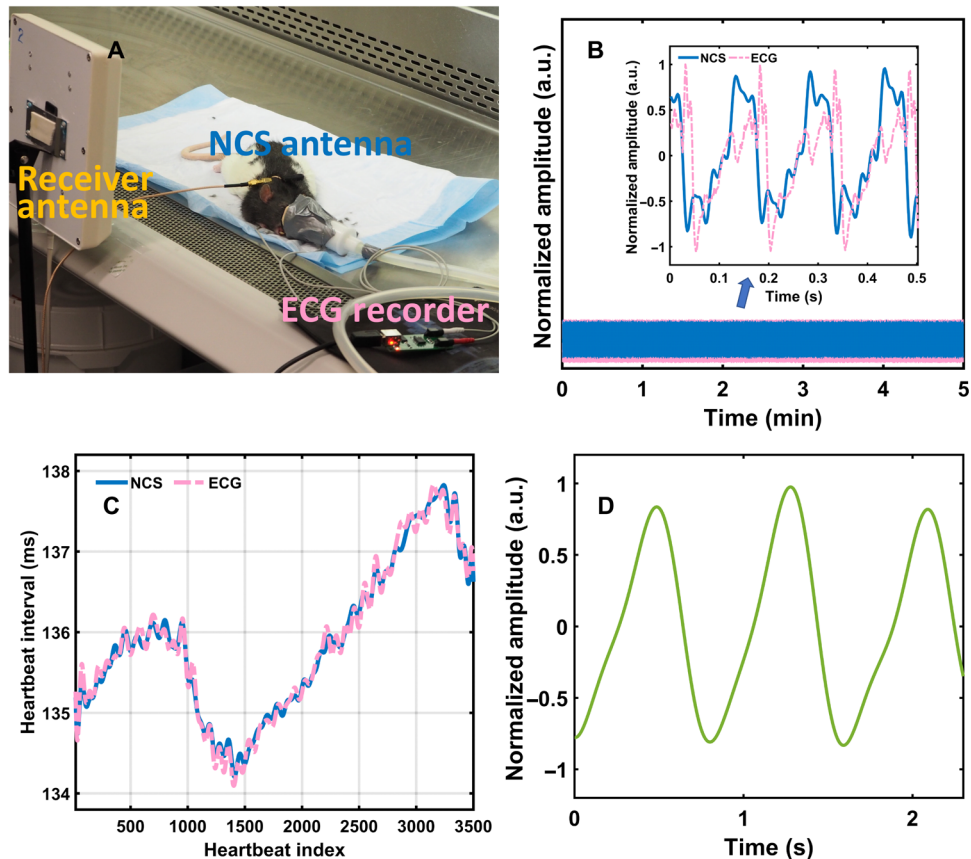
Fig. 2. The vital sign monitoring of a laboratory rat by synchronous NCS and ECG measurements. (**A**) Experimental setup with the anesthetized rat for ECG electrode placement. (**B**) Data recording (5 min) of NCS and ECG. The inset shows waveform details at a selected half-second duration. a.u., arbitrary units. (**C**) Heartbeat interval extracted from NCS and ECG showing very close match. (**D**) Representative respiration signals demodulated from the phase of the NCS signal around from the third to the fourth second. (The picture was taken by Xiaonan Hui, School of Electrical and Computer Engineering, Cornell University, Ithaca, NY 14853, USA.)

current further induced by the electrical heart stimulation and blood flow. In this perspective, NCS has a waveform transducing the heart internal and external mechanical motion, which is related to the mechanical information in ballistocardiogram (BCG) (*29*) and seismic cardiography (SCG) (*30*). In addition, NCS is much less subjected to variations from skin preparation steps and resulting surface conditions in comparison with ECG.

Other small conscious animals

After confirming the cardiopulmonary signals on the anesthetized rat, we next demonstrated the possible noninvasive NCS setups on several other species of small conscious animals, for which other monitoring methods such as ECG have been difficult, if not impossible (see Figs. 3 and 4). A pet golden hamster (*Mesocricetus*), named "Timo," was monitored in its cage sleeping quarter, as shown in Fig. 3A. Both wireless and wired NCS architectures in Fig. 1 were applied outside the cage. For the wireless version, the passive harmonic tag was powered up by the downlink signal, part of which was converted to the second harmonic as the NCS sensing signal coupled into the hamster body. The reader Rx antenna was about 1.5 m away from the tag. For the wired version, the sensing antenna was mounted on the right side of the sleeping quarter, which transmitted the NCS sensing signal directly. In Fig. 3B, the waveforms for respirations and heartbeats were acquired without the hamster being

aware of the device. The amplitudes of the vital signals were normalized to the maximum values of the entire recording period. The inset shows the heartbeat waveform details around the ninth second. The waveform features were similar not only for each heartbeat during the recording but also to those in the anesthetized rat in Fig. 2B. The negative minimums of the waveform were extracted for the heartbeat interval, as shown in Fig. 3C, after applying moving average with a window size of 20. The hamster heartbeat interval was about 20% longer than that of the rat.

We then continued the measurements when the hamster was running on the exercise wheel, as shown in Fig. 3D. The NCS sensing antenna was placed to the back of the wheel outside the cage, and the reader antenna is about 1.5 m away. The raw data from the demodulated NCS signal are shown as the red curve in Fig. 3E. From around 0 to 4 s and 12 to 20 s, the hamster was running on the wheel but otherwise took an intermittent rest without large body motion. After the bandpass filtering of 1 to 30 Hz, the time-domain signal is shown as the green curve in Fig. 3E, and the corresponding spectrum is shown in Fig. 3F. Because of the high heartbeat rate of the hamster, the heartbeat peak (blue arrow) and the derived heart rate can often be distinguished from the major body motion interference with different spectral content (black arrow). The second and third harmonic components of the heartbeat are also shown in the spectrum, indicated by the red and green arrows. An equalized peak
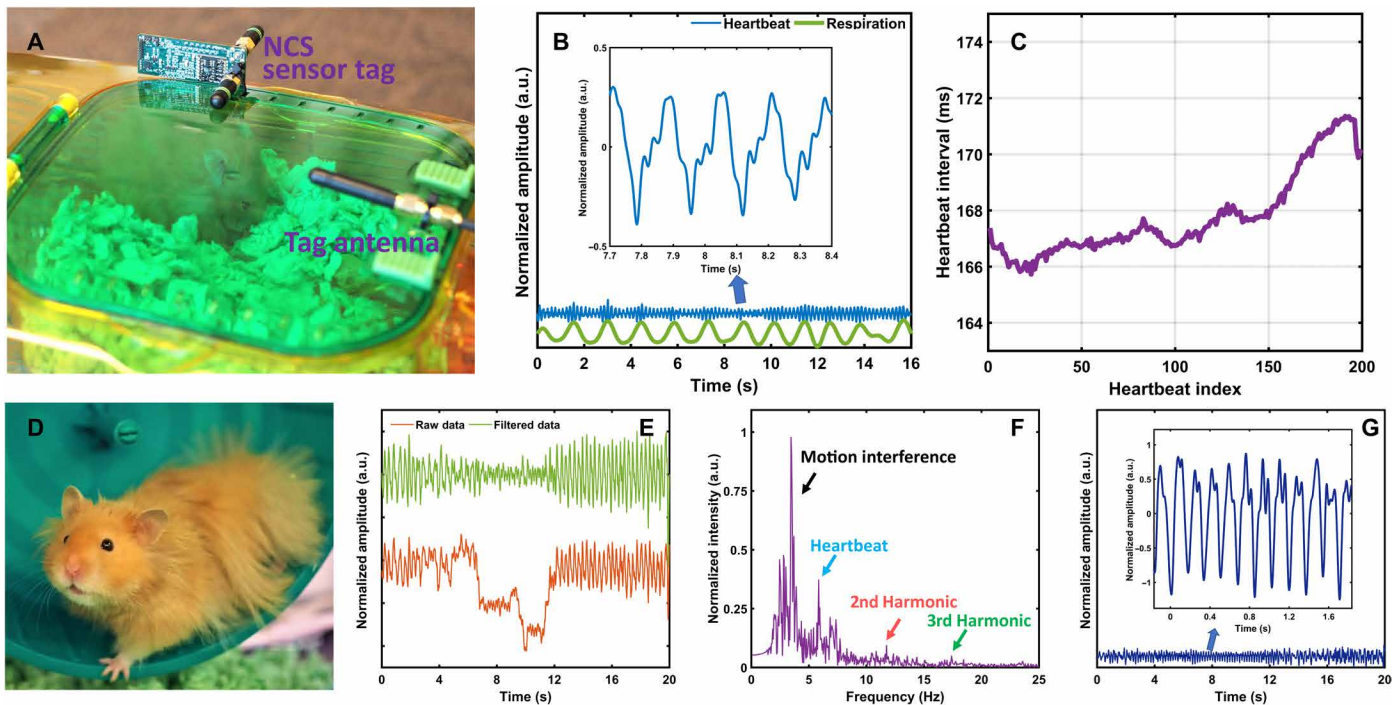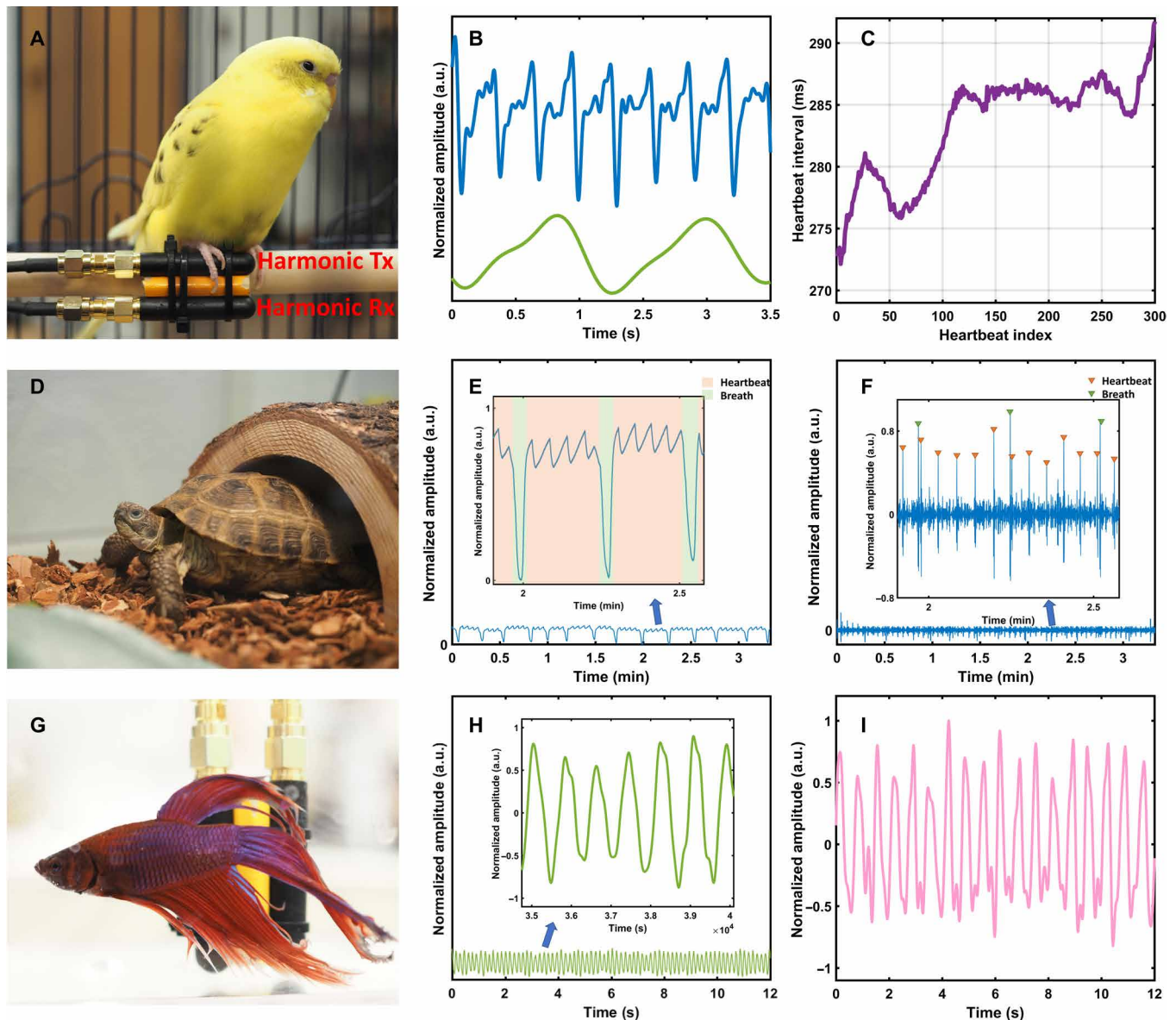
Fig. 3. The vital sign monitoring of a conscious pet hamster. (**A**) Illustrations of the experimental setup when the hamster was in its sleeping quarter. (**B**) Heartbeat (blue) and respiration (green) signals demodulated from NCS. The inset shows the heartbeat waveform details around the ninth second. (**C**) Heartbeat interval extraction for about 30 s. (**D**) Experimental setup when the hamster was running in the exercise wheel during the measurements. The NCS tag antenna was placed at the back of the wheel outside the wire cage. (**E**) Demodulated NCS raw data (red) and data after bandpass filtering (green) for 20 s. (**F**) The spectrum of the NCS signal indicates the frequency components of the body motion and the heartbeat as well as its harmonics. (**G**) Reconstructed time-domain heartbeat waveform after the equalized comb filtering. The inset shows the waveform details when the hamster was under the intermittent rest with less motion interference. (The pictures were taken by Xiaonan Hui, School of Electrical and Computer Engineering, Cornell University, Ithaca, NY 14853, USA.)

comb filter was then applied to recover the time-domain heartbeat waveform, as shown in Fig. 3G (21). The inset of Fig. 3G shows the waveform around the eighth second, when the hamster was under the intermittent rest. The sharp negative peaks can be detected for accurate heartbeat interval calculation. The heartbeat waveforms during the period of running still contained distortion from the strong motion artifact, where more advanced signal-processing methods are needed to obtain clearer results. Comb filtering can also be unreliable as a way to get rid of the NCS body motion interference when the motion in the near-field region has similar spectral content. In comparison, ECG had been attempted for free-moving conscious rodents by three paw pads (31). Recording is only valid when at least two pads are in touch with bare paws or body parts, which makes the pad design strongly dependent on the body shape and size. The rodent under test also needs to be moved from its habitat to the heated pad setup.

In addition to rodents, our touchless NCS method can be broadly administered to many other small conscious animals with various sizes, shapes, and body coverings. To demonstrate NCS applicability to small birds, we measured a pet fancy parakeet (*Melopsittacus undulates*, also known as budgies), named "Banana," as shown in Fig. 4 (A to C). Noninvasive monitoring of vital signs of conscious avian species will enable new capabilities in behavior studies, as well as health screening. Figure 4A demonstrates the wired experimental setup. The harmonic Tx antenna was fixed on the perch and transmitted the NCS sensing signal, which was coupled into the parakeet body. The harmonic Rx antenna was also integrated to the perch

and was able to acquire detailed features of both heartbeat and respiration, as shown in Fig. 4B, with the extracted heartbeat intervals in Fig. 4C. Movie S1 shows the real-time experiment. The blue and green curves on the screen represent the heartbeat and the breath waveforms, respectively. The antenna deployment was very convenient for the wired NCS setup. After simple observation of the parakeet behavior, we identified several positions on the perch where the bird usually stood. We chose the most frequent one and mounted the antenna pair. During the NCS measurement, there was no interference to the circadian rhythm of the parakeet.

The next demonstration was made on a pet Russian tortoise (*Agrionemys horsfieldii*, also known as Horsfield's tortoise or Central Asian tortoise), named "Blimp," as shown in Fig. 4 (D to F). Russian tortoises were the first vertebrate species to reach the moon orbits (32) and are important for studies of long space travels because of their sub-hibernation capability, which makes the continuous long-term recording of the vital signs even more scientifically important. Tortoises have a body structure of a hard shell and soft body tissues separated by small air gaps. Vital sign acquisition by ECG and ultrasound is only feasible with neck or intramuscular probes (5), both of which cause major discomfort to the animal. The physiological features of the shell and being ectothermic, together with the lack of proper diagnostic methods, have thus made chelonian critical care very difficult (33). The hearts of birds and rodents have four chambers with two atria and two ventricles, similar to human, and thus, the NCS waveforms in Figs. 2B, 3B, and 4B have similar features. In comparison, tortoises have a three-chamber heart consisting of two

Fig. 4. The vital sign monitoring of small conscious animals with noninvasive NCS setups. (**A**) Wired NCS setup for the parakeet. (**B**) Heartbeat (blue) and respiration (green) signals demodulated from NCS. (**C**) Extracted heartbeat intervals for about 1.5 min. (**D**) NCS setup for the Russian tortoise similar to Fig. 3A, where the antennas are under the wood chip flooring. (**E**) Normalized raw amplitude of the NCS signal for 3 min, which represents both breaths and heartbeats due to the shell structure. The inset shows the waveform details of the overlapped signals. The pink shaded sections indicate the heartbeats, while the green shaded sections indicate the breaths. The strong breath signal will overwhelm the heartbeat signal during the overlap. (**F**) The online processed signals during the same period as (E) by continuous wavelet transform (CWT) show clear separation of heartbeats and breaths for accurate rate estimation. The inset shows the extracted waveform details, indicating every peak in heartbeats and breaths. (**G**) NCS setup similar to Fig. 3A for the betta fish. The Tx and Rx antennas are deployed in the water close to the fish. (**H**) Demodulated NCS phase signal caused by the pectoral fin movement, where the inset shows the waveform details. (**I**) Demodulated NCS magnitude signal possibly caused by the heartbeat. (The pictures were taken by Xiaonan Hui, School of Electrical and Computer Engineering, Cornell University, Ithaca, NY 14853, USA.)

atria and one ventricle, and the NCS cardiogram has different features, although the heart rate can still be accurately retrieved. The NCS setup is shown in Fig. 4D. A similar antenna pair in Fig. 4A was placed under the cedarwood chips outside the glass cage. Due to the body structure, respiration and heartbeat signals were both embedded in the raw data of the NCS amplitude in Fig. 4E because there was no shell surface movement during breath. The heartbeat signal could sometimes be clear (as shown in the pink shaded regions in the inset) but would be overwhelmed by the strong breath signal during

the respiration movement (the green shaded regions) because of the relatively larger volume of the lungs. To separate the two overlapped signals for accurate rate estimation, the continuous wavelet transform (CWT) was used to extract the peak features of both waveforms in Fig. 4F. We have also tried the antenna placement directly on the vertebral shell and plastron, where the NCS heartbeat and respiration signals can be clearly recorded as well.

Last but not least, RF signals lower than a few gigahertz can propagate a short range in water with reasonably low attenuation,

especially for near-field coupling. Although ECG telemetry has been previously demonstrated (*34*), the instrument implant procedure is only suitable for larger fish with a week-long recovery period before unbiased measurements can be performed. Thus, ichthyologists have long sought after other noninvasive solutions to retrieve physiological information for behavior studies and evolution biology in small fish. We demonstrated the vital sign measurements of a pet betta splendens (*Betta channoides*, also known as Siamese fighting fish), named "Glee," in Fig. 4 (G to I). The demodulated NCS phase signal was interpreted as pectoral fin movement in Fig. 4G, which had a periodic waveform with frequency matched with the unsynchronized video recording. We hypothesized that the demodulated NCS magnitude signal in Fig. 4I represented the periodical waveform originated from the heartbeat. Because of the lack of other direct measurements for comparison, further studies are needed to confirm the motion source.

CONCLUSION

Here, we demonstrate a novel noninvasive method to measure the vital signs of small conscious animals, including furry mammals, birds, tortoises, and fish. Our NCS system with convenient setup not only provides the previously unachievable sensing capability but also improves the animal testing protocols with no harm to their welfare or interference to their circadian rhythms. Previous preparation methods for vital sign monitoring such as anesthetization, hair removal, alligator clips, intramuscular probe insertion, shell hole drilling, and body implant can all be avoided. Our demonstrations can be further adapted to other species and laboratory settings to provide more humane study, care, and assessment of animals; our method also provides measurement of unbiased vital signs of animals monitored in their natural state.

MATERIALS AND METHODS

Hardware configuration

As shown in Fig. 1, the harmonic reader is implemented by an SDR consisting of Ettus USRP X310 and UBX 160 MHz RF daughterboards (*35*). Ettus USRP B200/210 can also be configured as the harmonic reader for this application, but X310 has higher data sampling rates for high resolution of waveform details. To function as a coherent harmonic transceiver in Fig. 1, the Tx chain (the blue triangle) and the Rx chain (the orange triangle) share the same RF clock source (the yellow circle). The synthesizer in the Rx chain configures the local oscillator (LO) frequency at two times of the Tx LO frequency. The Tx baseband (the gray arrow) is generated by the field-programmable gate array (FPGA), while the Rx baseband is fed into FPGA to be demodulated for data recording and display.

Both wireless and wired versions in Fig. 1 can be applied for NCS. In the wireless version in Fig. 1A, the passive harmonic tag (*36*) was modified from the wireless identification and sensing platform (WISP) (*37*), with the addition of the nonlinear transmission line (NLTL) and data modulation on the second-harmonic backscattering signal (*38*). NLTL is a ladder structure of inductors and varactors, so the varactor symbol is chosen to represent the harmonic tag and harmonic generator. The harmonic tags were operated under harvested RF power and can be readily deployed in large quantities (*25*) on many sensing targets or on multiple points of the same target (*22*). Alternatively, for single-point monitoring, the wired version in

Fig. 1B is easier to apply to indoor animal laboratories. The harmonic generator here can still be NLTL as before to provide high-conversion efficiency over a broad band (*38*). The low-pass filter at the input port isolates the direct harmonic reflection from NLTL to the reader, and the high-pass filter at the output port of the NLTL damps out the signal at the fundamental frequency to the Tx antenna. Unlike the tight power constraint in the passive tag, any active or passive frequency doubler with proper frequency response can replace the NLTL in the wired version. During the experiments, we tried the custom diodes and commercial passive doubler (CRYSTEK CPPD-0.85-2) as the harmonic generator, both of which provided satisfactory performance. The wired NCS system can also be extended for multiple points with the reader CDMA technique (*39*), but the system cost will increase proportionally. The benefits of the harmonic system were demonstrated in our pervious works (*22*, *24*, *25*). In short, the harmonic system provides much better isolation between Tx and Rx, so the Rx noise floor can be much lower to improve both SNR and reader Rx sensitivity. In turn, the Tx power can also be tuned lower to still maintain sufficient SNR for the vital sign sensing, which eliminates any further health concern about the RF power impinging to live tissues.

Software configuration

The SDR is controlled by the computer with LabVIEW. The sampling rates of the DAC (digital-to-analog converter) and ADC (analog-to-digital converter) are both configured at 10 MSps (mega-samples per second). The frequency of the baseband output from the DAC is 1 MHz. When the Tx LO frequency is 950 MHz, the signal output from the Tx is 951 MHz. After the harmonic conversion, the center frequency of the Rx signal will be around 1902 MHz. The Rx LO at 1900 MHz is set to be two times of the Tx LO. Hence, the Rx baseband frequency is 2 MHz to be sampled by the ADC. The digitized baseband signal is down-converted and down-sampled in LabVIEW to an NCS sampling rate of 5 kSps (kilo-samples per second).

SUPPLEMENTARY MATERIALS

REFERENCES AND NOTES

1. P. P. Pereira-Junior, M. Marocolo, F. P. Rodrigues, E. Medei, J. H. M. Nascimento, Noninvasive method for electrocardiogram recording in conscious rats: Feasibility for heart rate variability analysis. *An. Acad. Bras. Cienc.* **82**, 431–437 (2010).

2. R. H. Wolf, N. D. Lehner, E. C. Miller, T. B. Clarkson, Electrocardiogram of the squirrel monkey, *Saimiri sciureus*. *J. Appl. Physiol.* **26**, 346–351 (1969).

3. E. Lepeschkin, B. Surawicz, The measurement of the Q-T interval of the electrocardiogram. *Circulation* **6**, 378–388 (1952).

4. P. Kligfield, L. S. Gettes, J. J. Bailey, R. Childers, B. J. Deal, E. W. Hancock, G. van Herpen, J. A. Kors, P. Macfarlane, D. M. Mirvis, O. Pahlm, P. Rautaharju, G. S. Wagner, Recommendations for the standardization and interpretation of the electrocardiogram: Part I: The electrocardiogram and its technology: A scientific statement from the American Heart Association Electrocardiography and Arrhythmias Committee, Council on Clinical Cardiology; the American College of Cardiology Foundation; and the Heart Rhythm Society endorsed by the International Society for Computerized Electrocardiology. *Circulation* **115**, 1306–1324 (2007).

5. A. E. Bowles, S. Eckert, L. Starke, E. Berg, L. Wolski, *Effects of Flight Noise From Jet Aircraft and Sonic Booms on Hearing, Behavior, Heart Rate and Oxygen Consumption of Desert Tortoises* (Gopherus agassizii) (United States Air Force Research Laboratory, 1999).

6. J. Allen, Photoplethysmography and its application in clinical physiological measurement. *Physiol. Meas.* **28**, R1–R39 (2007).

7. T. Tamura, Y. Maeda, M. Sekine, M. Yoshida, Wearable photoplethysmographic sensors—Past and present. *Electronics* **3**, 282–302 (2014).

8. J. R. Kindig, T. P. Beeson, R. W. Campbell, F. Andries, M. E. Tavel, Acoustical performance of the stethoscope: A comparative analysis. *Am. Heart J.* **104**, 269–275 (1982).

9. H. Liang, S. Lukkarinen, I. Hartimo, Heart sound segmentation algorithm based on heart sound envelogram, *Proceedings of the 1997 IEEE Computers in Cardiology*, Lund, Sweden, 7 to 11 September 1997.

10. P. J. A. Frinking, A. Bouakaz, J. Kirkhorn, F. J. Ten Cate, N. de Jong, Ultrasound contrast imaging: Current and new potential methods. *Ultrasound Med. Biol.* **26**, 965–975 (2000).

11. J. S. Mattoon, T. G. Nyland, *Small Animal Diagnostic Ultrasound* (Elsevier Health Sciences, 2014).

12. J. C. Lin, Noninvasive microwave measurement of respiration. *Proc. IEEE* **63**, 1530 (1975).

13. C. Li, V. M. Lubecke, O. Boric-Lubecke, J. Lin, A review on recent advances in Doppler radar sensors for noncontact healthcare monitoring. *IEEE Trans. Microwave Theory Techn.* **61**, 2046–2060 (2013).

14. C. Li, Z. Peng, T.-Y. Huang, T. Fan, F.-K. Wang, T.-S. Horng, J.-M. Muñoz-Ferreras, R. Gómez-García, L. Ran, J. Lin, A review on recent progress of portable short-range noncontact microwave radar systems. *IEEE Trans. Microw. Theory Tech.* **65**, 1692–1706 (2017).

15. F. Adib, H. Mao, Z. Kabelac, D. Katabi, R. C. Miller, Smart homes that monitor breathing and heart rate, *CHI '15 Proceedings of the 33rd Annual ACM Conference on Human Factors in Computing Systems*, Seoul, Korea, 18 to 23 April 2015.

16. F. Pfanner, T. Allmendinger, T. Flohr, M. Kachelrieß, Modelling and simulation of a respiratory motion monitor using a continuous wave Doppler radar in near field, *Proceedings of the Medical Imaging 2013: Physics of Medical Imaging, International Society for Optics and Photonics*, Lake Buena Vista, FL, 6 March 2013.

17. T.-Y. Huang, J. Lin, L. F. Hayward, Non-invasive measurement of laboratory rat's cardiorespiratory movement using a 60-GHz radar and nonlinear Doppler phase modulation, *Proceedings of the 2015 IEEE MTT-S International Microwave Workshop Series on RF and Wireless Technologies for Biomedical and Healthcare Applications (IMWS-BIO)*, Taipei, Taiwan, 21 to 23 September 2015.

18. T.-Y. Huang, L. F. Hayward, J. Lin, Noninvasive measurement and analysis of laboratory rat's cardiorespiratory movement. *IEEE Trans. Microw. Theory Tech.* **65**, 574–581 (2017).

19. A. Serra, R. Reggiannini, R. Massini, P. Nepa, RF sensor for non-invasive cardiopulmonary monitoring, *Proceedings of the International Conference on Wireless Mobile Communication and Healthcare*, Paris, France, 21 to 23 November 2012.

20. R. R. G. Perron, M. F. Iskander, T. B. Seto, G. C. Huang, D. A. Bibb, Electromagnetics in medical applications: The cardiopulmonary stethoscope journey, in *World of Applied Electromagnetics* (Springer, 2017), pp. 443–479.

21. N. Celik, R. Gagarin, G. C. Huang, M. F. Iskander, B. W. Berg, Microwave stethoscope: Development and benchmarking of a vital signs sensor using computer-controlled phantoms and human studies. *IEEE. Trans. Biomed. Eng.* **61**, 2341–2349 (2014).

22. X. Hui, E. C. Kan, Monitoring vital signs over multiplexed radio by near-field coherent sensing. *Nat. Electron.* **1**, 74–78 (2018).

23. X. Hui, E. C. Kan, Mitigation of body movement interference in near-field coherent sensing for heartrate monitoring, *Proceedings of the IEEE 15th International Conference on Wearable and Implantable Body Sensor Networks (BSN) 2018*, Las Vegas, NV, 4 to 7 March 2018.

24. Y. Ma, X. Hui, E. C. Kan, 3D real-time indoor localization via broadband nonlinear backscatter in passive devices with centimeter precision, *Proceedings of the 22nd Annual International Conference on Mobile Computing and Networking (MobiCom'16)*, New York City, NY, 3 to 7 October 2016.

25. X. Hui, Y. Ma, E. C. Kan, Code division multiple access in centimeter accuracy harmonic RFID locating system. *IEEE J. Radio Freq. Identif.* **1**, 51–58 (2017).

26. National Research Council, Animal and human studies addressing health effects, in *An Assessment of Potential Health Effects from Exposure to PAVE PAWS Low-Level Phased-Array Radiofrequency Energy* (The National Academies Press, 2005), chap. 7.

27. M. Bolić, D. Simplot-Ryl, I. Stojmenović, *RFID Systems: Research Trends and Challenges* (Wiley, 2010).

28. P. H. Gordon, R. Chen, H. Park, E. C. Kan, Embroidered antenna characterization for passive UHF RFID tags. arXiv:1710.02237 [eess.SP] (5 October 2017).

29. E. Pinheiro, O. Postolache, P. Girão, Theory and developments in an unobtrusive cardiovascular system representation: Ballistocardiography. *Open Biomed. Eng. J.* **4**, 201–216 (2010).

30. O. T. Inan, P.-F. Migeotte, K.-S. Park, M. Etemadi, K. Tavakolian, R. Casanella, J. Zanetti, J. Tank, I. Funtova, G. K. Prisk, M. Di Rienzo, Ballistocardiography and seismocardiography: A review of recent advances. *IEEE J. Biomed. Health Inform.* **19**, 1414–1427 (2015).

31. ECGenie Video, How to record ECG non-invasively in conscious mice; https://mousespecifics.com/heart-monitoring/ECGenie-video.

32. A. C Madrigal, "Who was first in the race to the moon? The tortoise," *The Atlantic*, 27 December 2012.

33. T. M. Norton, Chelonian emergency and critical care. *Semin. Avian Exot. Pet. Med.* **14**, 106–130 (2005).

34. V. J. T. van Ginneken, P. Snelderwaard, R. van der Linden, N. van der Reijden, G. E. E. J. M. van den Thillart, K. Kramer, Coupling of heart rate with metabolic depression in fish: A radiotelemetric and calorimetric study. *Thermochim. Acta* **414**, 1–10 (2004).

35. USRP X310 and UBX-160 daughterboard, products of Ettus Research (2018); https://www.ettus.com/product.

36. Y. Ma, X. Hui, E. C. Kan, Harmonic-WISP: A passive broadband harmonic RFID platform, *Proceedings of the 2016 IEEE MTT-S International Microwave Symposium (IMS)*, San Francisco, CA, 22 to 27 May 2016.

37. D. J. Yeager, A. P. Sample, J. R. Smith, WISP: A passively powered UHF RFID tag with sensing and computation, in *RFID Handbook: Applications, Technology, Security, and Privacy* (CRC Press, 2008), pp. 261–278.

38. F. Yu, K. G. Lyon, E. C. Kan, A novel passive RFID transponder using harmonic generation of nonlinear transmission lines. *IEEE Trans. Microw. Theory Tech.* **58**, 4121–4127 (2010).

39. X. Hui, E. C. Kan, Collaborative reader code division multiple access in the harmonic RFID system. *IEEE J. Radio Freq. Identif.* **2**, 86–92 (2018).

Citation: X. Hui, E. C. Kan, No-touch measurements of vital signs in small conscious animals. *Sci. Adv.* **5**, eaau0169 (2019).